Inclusive neutron spectra at 0° from Nb-Nb and Au-Au collisions at 800 MeV/nucleon

R. Madey, W.-M. Zhang, B. D. Anderson, A. R. Baldwin, B. S. Flanders,* W. Pairsuwan,†
J. Varga, and J. W. Watson
Kent State University, Kent, Ohio 44242

G. D. Westfall
Michigan State University, East Lansing, Michigan 44823
(Received 29 February 1988)

Inclusive neutron spectra were measured at 0° from Nb-Nb and Au-Au collisions at 800 MeV/nucleon. The spectra in the rest frame of the projectile were decomposed into three Gaussians with standard deviations of 55±4, 114±12, and 259±22 MeV/c for Nb-Nb collisions, and 56±4, 110±10, and 279±15 MeV/c for Au-Au collisions. Physical processes associated with each Gaussian are discussed. The dependence of the parameters of the three Gaussians on the impact parameter indicates that the temperature of the spectators excited by peripheral collisions is lower than that excited by nonperipheral collisions, that projectile neutrons involved in nonperipheral collisions have a broader momentum distribution than those involved in peripheral collisions, and that an observed high-energy tail has its origin primarily in nonperipheral collisions. The high-energy tail is explained well by collective backscattering of neutrons in the target from nucleon clusters in the projectile with a mean cluster size of about 1.3 in both Nb and Au.

I. INTRODUCTION

Heavy-ion experiments have provided new information about nuclear structure; with increasing beam energy, these experiments offer a way to produce hotter and denser nuclear matter in the laboratory for further study. A statistical model, introduced by Feshbach and Huang[1] and extended by Goldhaber,[2] was used to interpret the projectile-fragmentation measurements of Heckman *et al.*[3] Feshbach and Huang relate the Fermi momentum P_F of a nucleon in the projectile to the standard deviation σ of a Gaussian representation of the Lorentz-invariant cross section spectrum at 0° in the rest frame of the projectile. Alternatively, by assuming a postcollision equilibration, Goldhaber relates this σ to the temperature of a thermal system. Inclusive neutron spectra at 0° from Ne-NaF and Ne-Pb collisions at 390 and 790 MeV/nucleon were reported earlier.[4] Those spectra in the rest frame of the projectile were decomposed into three Gaussians. It was suggested that the narrowest Gaussian originated from the thermal process of evaporation of neutrons from the projectile nucleus at a certain temperature; the Gaussian of intermediate width was interpreted as arising from an impulsive collision that samples the Fermi momentum of a neutron in the projectile nucleus; and possible origins mentioned for the broadest Gaussian included collective behavior from central collisions, a high-energy tail of the Fermi distribution of nucleons in the projectile nucleus at a finite temperature, and collective backscattering of a neutron in the target from a cluster of nucleons in the projectile.

In this paper, we report measurements of inclusive neutron spectra at 0° from 800 MeV/nucleon collisions of Nb ions on a Nb target and Au ions on a Au target. For each projectile-target system, the Lorentz-invariant cross section in the rest frame of the projectile was decomposed into three Gaussians as in the analysis of the earlier experiment mentioned previously. In this experiment, we examined also the dependence of the Lorentz-invariant cross section on the impact parameter, the distribution of the transverse momentum of the neutrons at 0°, and the downshift in the peak momentum of the neutrons. The results from this experiment show again the existence of three processes of neutron emission and support the previous interpretations for the sources of the first and second Gaussians, and provide additional information in support of the explanation that the third Gaussian arises from elastic scattering of a neutron in the target from a cluster of nucleons in the projectile.

II. APPARATUS

The data were taken at the Bevalac accelerator at the Lawrence Berkeley Laboratory. Nine mean-timed[5] neutron detectors[6] were installed at 0°, 4°, 8°, 15°, 30°, 42°, 90°, 120°, and 160° with respect to the beam direction. In this paper, we discuss the measurements from the detector at 0°, which was an NE-102 plastic scintillator, 10.16 cm thick, 101.6 cm high, and 25.4 cm wide. It detected neutrons from collisions of Nb (Au) on Nb (Au) with a projectile energy of 800 MeV/nucleon at the center of a 1.37 gm/cm^2 Nb (1.71 gm/cm^{2}Au) target oriented at an angle of 45° with respect to the beam direction. Charged particles incident on the neutron detector were vetoed with a 6.4 mm thick plastic scintillation counter. The time of flight (TOF) of each detected neutron was determined by measuring the time difference between the detection of the neutron and the detection of a Nb (or Au) ion in a beam telescope, which consisted of two NE-102 (76.2 mm×76.2 mm×0.8 mm thick) scintillation counters positioned upstream of the target. Based

on the calibration of the time-to-amplitude converter module, one TOF channel was equivalent to 93.3 ps. With an observed standard deviation of 390±70 ps [half-width at half maximum (HWHM)=460±83 ps] in the time resolution as shown in Fig. 1, the standard deviation in the energy resolution was estimated to be 33±6 MeV for an 800 MeV neutron over a 14.3 m flight path. Note that the energy resolution associated with the HWHM of 460±83 ps is 39±7 MeV. The neutron detection efficiencies, as calculated with the Monte Carlo code of Cecil *et al.*,[7] varied from 7.4% at 150 MeV to 3.8% above 2 GeV with a proton energy threshold of 20 MeV. Calculations of neutron detection efficiencies with this code agree with measured efficiencies for both plastic and liquid hydrocarbon scintillators for neutron energies from 1 MeV to about 300 MeV, and for detector thresholds from 0.1 MeV to 22 MeV equivalent-electron energies. Additional tests of these calculated efficiencies were made by comparing various (p,n) and (p,p') analog reactions up to about 500 MeV.[8–11]

The intensity of the usable incident beam was about 2×10^5 ions per pulse after a rejection loss of about 60%. The beam pulse was spilled for about 0.5 sec every 5 sec for the Nb beam and every 4 sec for the Au beam. After traversing the beam telescope and the target, the beam was deflected by the large aperture heavy-ion spectrometer system (HISS) magnet through an angle of 15° into a reentrant beam dump. A large (177.8 cm high×101.6 cm wide×0.95 cm thick) scintillation counter was located in front of the beam dump. The pulse height from this centrality detector served as a monitor for the impact parameter of the collisions.

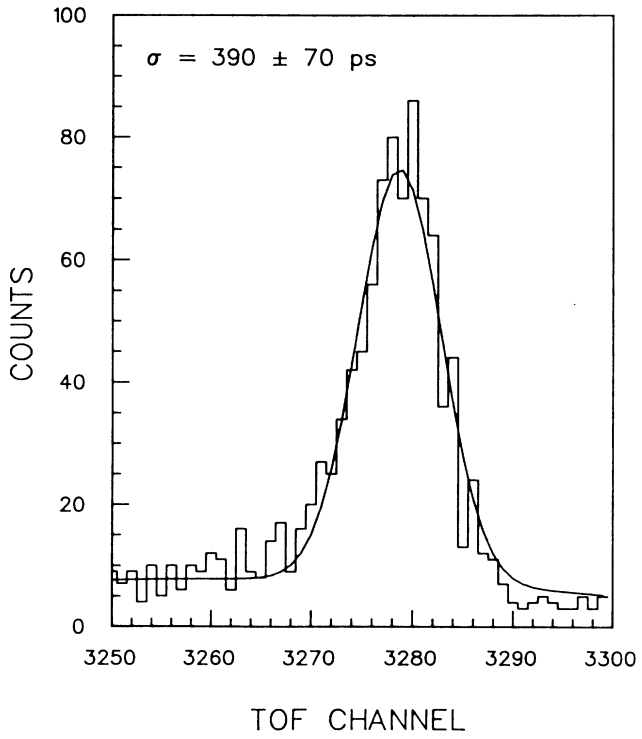

FIG. 1. A typical TOF histogram of gamma rays emitted from Au-Au collisions at 800 MeV/nucleon. The Gaussian fit above background has a standard deviation of 4.2±0.7 TOF channels, which corresponds to a time resolution of 390±70 ps with a calibration of 93.3 ps per TOF channel.

Target-correlated background was determined from measurements with and without a steel shadow shield, 152.4 cm long by 71.1 cm high by 20.3 cm wide, with the front face located 6 m away from the target. The shadow shield attenuated neutrons by a factor greater than 10^4 at all energies.

III. INCLUSIVE SPECTRA

The kinetic energy of each detected neutron was obtained from the measured TOF. The cross sections were calculated from the number of neutrons counted in the 0° detector after subtracting a small number of coincidences with any other detector. Events with two neutrons in the 0° detector were indistinguishable from single-neutron events. The cross sections were corrected for the relatively small number of these two neutron events by a multiplicative factor of $(1+R)$, where R is the ratio of the number of two-neutron events to the number of noncoincident events in the 0° detector. Because the detectors at 0° and 4° subtend the same solid angle, this ratio $R \simeq R_0/2$, where R_0 is the ratio of the number of coincident events between the detectors at 0° and 4° to the number of noncoincident events in the detector at 0°. The ratio R_0 was observed to be about 22±4 % for Au-Au collisions and 5±1 % for Nb-Nb collisions; within uncertainties, this ratio did not vary significantly in an auxiliary test with Au-Au collisions when the 4° detector was moved adjacent to the 0° detector, and it was approximately the same for both peripheral and nonperipheral collisions as defined later in this paper. The ratio R_0 for each system is consistent with the expectation that it is approximately proportional to the square of the number of neutrons in the nucleus, provided that the product of the detection efficiency and the number of neutrons striking the detector is smaller than and not close to unity. The observed relatively low values for the ratio R_0 for both Au-Au and Nb-Nb collisions confirm that this product is small and guarantee the validity of the approximation.

Inclusive double-differential cross sections at 0° are plotted in Fig. 2 as a function of the neutron laboratory kinetic energy for both Nb-Nb and Au-Au collisions. The spectra are characterized by a high-energy tail and a strong peak at a neutron energy of about 753 MeV for Nb-Nb collisions and 731 MeV for Au-Au collisions. These energies are slightly below the beam energy per nucleon. The high-energy tail extends beyond the kinematic limit for free nucleon-nucleon scattering; that is, two-body collisions of nucleons with Fermi momenta appropriate to nucleons in a cold target and a cold projectile cannot account for neutrons in the high-energy region. The kinematic limit is much lower than the energy of neutrons in the high-energy tail; for a Fermi momentum of about 260 MeV/c, it is estimated to be about 1.03 GeV for Nb-Nb and Au-Au collisions at 800 MeV/nucleon.

The uncertainties shown in Fig. 2 include both the

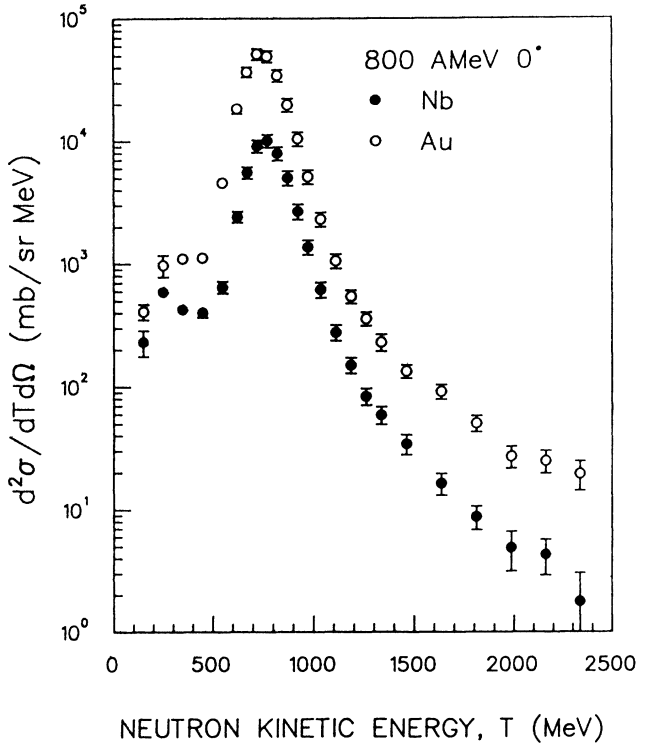

FIG. 2. The inclusive double differential cross section at 800 MeV/nucleon for neutron emission at 0° from Nb-Nb (solid circles) and Au-Au (open circles) collisions vs the neutron kinetic energy in the laboratory.

statistics and the systematics. The uncertainties are dominated by the systematics of around 10% at a neutron energy below 800 MeV. The statistical uncertainty increases with increasing neutron energy. At a neutron energy of 2.3 GeV, the statistical uncertainty is approximately equal to the systematic uncertainty of about 18% for Au-Au collisions; at 2.3 GeV, the statistical uncertainty is as large as 60% for Nb-Nb collisions. The systematic uncertainties are dominated by the uncertainty arising from the choice of the proton energy threshold. The cross sections were calculated with a proton energy threshold of 20 MeV. Cross sections calculated with proton energy thresholds in the range from 12 to 28 MeV are more stable than those extracted with thresholds outside this range. For thresholds higher than 28 MeV, the uncertainty in the neutron detection efficiency becomes large; for thresholds lower than 12 MeV, background contamination from low-energy neutrons introduces a large uncertainty in the cross sections. Plotted in Fig. 3 for Nb-Nb collisions are the neutron detection efficiency, the neutron counts, and the cross section, normalized to the corresponding reference values at a proton energy threshold of 20 MeV, versus the proton energy threshold in the region from 12 to 28 MeV for several neutron energies from 200 MeV to 2.3 GeV. The relative stability in the cross section with proton energy thresholds in the region from 12 to 28 MeV demonstrates that neutron detection efficiencies at energies below 400 MeV are self-consistent for thresholds in this region. The fluctuations of the cross section with proton energy thresholds from 12 to 28 MeV for neutron energies above 1400 MeV results in large uncertainties in quantities associated with the high-energy tail in the spectra in Fig. 2; however, as we will see, these uncertainties do not prevent us from extracting physics results of interest.

The Lorentz-invariant cross sections are plotted in Figs. 4(a) and 5(a) for Nb-Nb and Au-Au collisions, respectively, as a function of P, the momentum of the neutron in the rest frame of the projectile. These two spectra span the momentum region from minus 200 to 730 MeV/c, which corresponds to the energy region of 530 MeV to 2.4 GeV in the laboratory. Each spectrum was decomposed into three Gaussians of the form

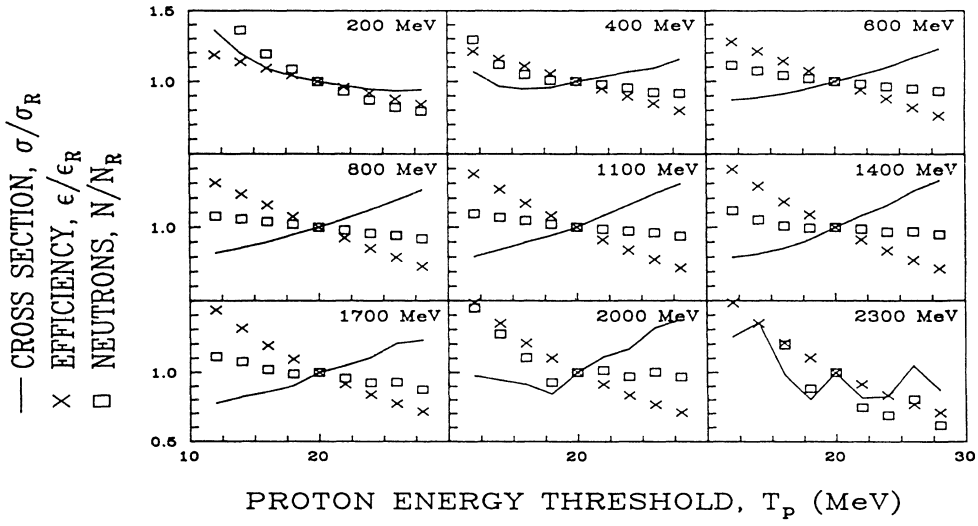

FIG. 3. Normalized neutron detection efficiency, neutron counts, and double differential cross section vs the proton energy threshold for neutron energies from 200 MeV to 2.3 GeV. Plotted quantities were normalized to values at a proton energy threshold of 20 MeV.

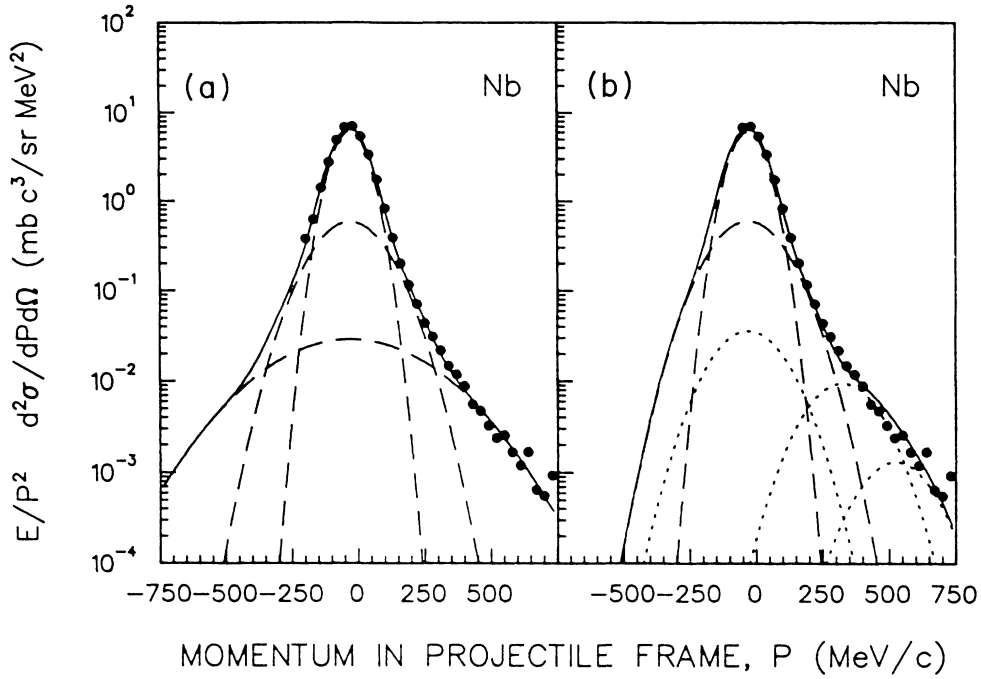

FIG. 4. The Lorentz-invariant cross section at 800 MeV/nucleon for neutron emission at 0° from Nb-Nb collisions vs the neutron momentum in the rest frame of the projectile. (a) displays the decomposition into three Gaussians. (b) displays the first two Gaussians and the three components of the third Gaussian.

$$(2\pi\sigma^2)^{-1/2}H\exp[-(P-P_0)^2/2\sigma^2]\ ,$$

which we associate with three processes of neutron emission. The decomposition was carried out by a fit that varied the standard deviation σ, the mean momentum P_0, and the amplitude H of each Gaussian. Note that the amplitude is equal to the integral or area of the Gaussian; i.e.,

$$H=\int_{-\infty}^{+\infty}(2\pi\sigma^2)^{-1/2}H\exp[-(P-P_0)/2\sigma^2]dP\ .$$

The mean momentum values of the Gaussians were con-

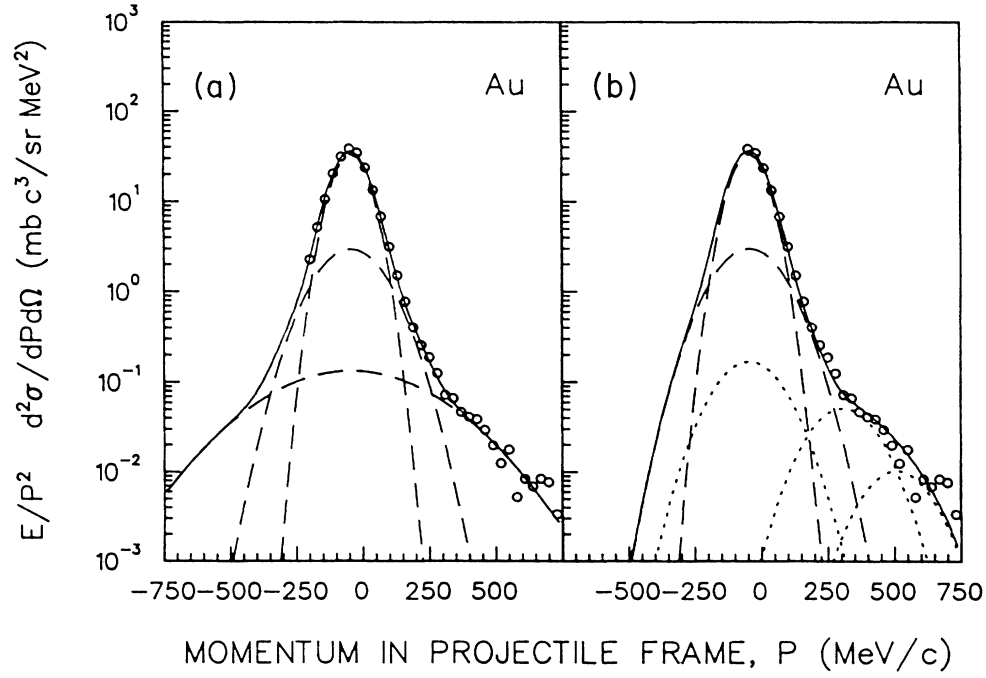

FIG. 5. The Lorentz-invariant cross section at 800 MeV/nucleon for neutron emission at 0° from Au-Au collisions vs the neutron momentum in the rest frame of the projectile. (a) displays the decomposition into three Gaussians. (b) displays the first two Gaussians and the three components of the third Gaussian.

strained to be the same in the fit. The χ^2 per degree of freedom of the fit was $6.4/25=0.26$ and $18.6/25=0.75$ for Nb-Nb and Au-Au collisions, respectively. In each of the two figures, the circles display the spectrum, the solid line represents the fit to the spectrum, and the dashed lines represent the decomposition of the spectrum into three Gaussians. The Gaussian with the smallest amplitude is not negligible, even with a large uncertainty in its amplitude of 39% for Nb-Nb collisions and 22% for Au-Au collisions; although this third Gaussian could be replaced by other forms, such as a polynomial or an exponential, these other forms would not differ much from a Gaussian with such large uncertainties. The results of fitting the data with only two Gaussians yielded a χ^2 per degree of freedom of $34.9/27=1.3$ and $69.5/27=2.6$ for Nb-Nb and Au-Au collisions, respectively; these larger values of χ^2 per degree of freedom indicate that the fit with two Gaussians is not as good as the fit with three Gaussians. The results of the fit with three Gaussians are summarized in Table I. The uncertainties include both the statistics and the systematics. The systematics are dominated by the uncertainty in the neutron detection efficiency and the uncertainty arising from the choice of the low edge of the fitting region. A low edge of minus 200 MeV/c was chosen to include the maximum amount of data and to exclude distortions from processes other than the three mentioned previously. Varying the low edge from -200 to -80 MeV/c, which is slightly below the mean momentum P_0, affected the results by only a few percent. Because the Monte Carlo code of Cecil *et al.*[7] does not include pion channels, the detection efficiency for neutrons above 500 MeV may be underestimated as shown by Jeppeson.[12] We examined the possibility that a higher neutron detection efficiency would affect our measurements, especially for the high-energy tail. If we change the neutron detection efficiencies from the code of Cecil *et al.* by a factor that increases linearly from 1.0 at a neutron energy of 500 MeV to 1.3 at a neutron energy of 2.3 GeV, the results of our measurement do not change within the uncertainties; also, the decomposition into three Gaussians yields standard deviations and amplitudes that differ from those in Table I by less than the stated uncertainties.

The magnitude of the mean momentum P_0 listed in Table I shows quantitatively the downshift ΔP in the peak momentum of the Gaussians relative to zero momentum in the projectile rest frame. After unfolding the momentum resolution, which has a standard deviation of 19±3 MeV/c at the mean momentum P_0, the standard deviations σ_1^*, σ_2^*, and σ_3^* of the three Gaussians were extracted to be 55±4, 114±12, and 259±22 MeV/c for Nb-Nb collisions and 56±4, 110±10, and 279±15 MeV/c for Au-Au collisions. These unfolded values are listed in the last column of Table I. If we release the constraint on the value of the mean momentum of the third Gaussian for both Nb-Nb and Au-Au collisions, the value of σ_3^* obtained from such a fit is unchanged within uncertainties; however, there is a very large uncertainty of about 150 MeV/c in the value of the mean momentum of the third Gaussian.

As suggested earlier,[4] the source of the first Gaussian is a thermal process of neutron evaporation after excitation of the projectile nucleus. To obtain the neutron evaporation temperature T_e, we used the formula derived by Goldhaber[2] for an equilibrated system: $\sigma^2 = MkT_eK(A-K)/A$, where σ is the standard deviation of a Gaussian, M is the mass of the nucleon, k is the Boltzmann constant, and K and A are the mass numbers of the fragment (i.e., the neutron here) and the projectile, respectively. We extracted evaporation temperatures of 3.3±0.5 and 3.4±0.5 MeV for Nb-Nb and Au-Au collisions, respectively, which agree with each other, and, within uncertainties, with the value of 2.7±0.4 MeV obtained for Ne-NaF and Ne-Pb collisions at 390 MeV/nucleon and 790 MeV/nucleon.[4] (The value 3.7 MeV quoted in Ref. 4 for this latter evaporation temperature was overestimated because it was based on the standard deviation obtained before unfolding the momentum resolution.) In terms of the parameters of the first Gaussian, the total cross section of the first process for evaporation of neutrons was estimated to be $2\pi H_1(\sigma_1^2+P_0^2)/\bar{E}$, where $\bar{E}$ ($\simeq$955 MeV) is the average total (rest mass + kinetic) energy of an evaporation neutron in the rest frame of the projectile; accordingly, the total cross section for evaporation of neutrons from the projectile is 26±3 and 174±19 b for Nb-Nb and Au-Au collisions, respectively.

The physical quantity extracted from the second

TABLE I. Parameters of the three Gaussians in the decomposition of the neutron spectra at 0° in the rest frame of the projectile from Nb-Nb and Au-Au collisions at 800 MeV/nucleon.

System	Gaussian	Peak momentum P_0 (MeV/c)	Standard deviation σ (MeV/c)	Amplitude H (mb c^2/sr MeV)	Standard deviation[a] σ^*(MeV/c)
Nb-Nb	1	−30±5	58±3	883±80	55±4
	2	−30±5	116±11	166±61	114±12
	3	−30±5	260±22	18±7	259±22
Au-Au	1	−44±4	59±3	4423±370	56±4
	2	−44±4	112±9	747±262	110±10
	3	−44±4	280±15	84±18	279±15

[a]σ^* is the standard deviation after unfolding the momentum resolution with a standard deviation of 19±3 MeV/c at the mean momentum P_0.

Gaussian was the Fermi momentum P_F. From the relation $\sigma^2=\frac{1}{5}P_F^2$ given explicitly by Goldhaber,[2] we determined the Fermi momentum P_F from the resolution-unfolded standard deviation σ_2^* to be 255±27 and 246±22 MeV/c for Nb and Au, respectively. Within uncertainties, these two values agree with the results from quasielastic electron scattering reported by Moniz *et al.*:[13] $P=254\pm5$ MeV/c for ^{89}Y and 265±5 MeV/c for ^{208}Pb.

A. Downshift in the peak momentum

The downshift in the peak momentum of the neutrons depends on the system and on the beam energy per nucleon. Listed in Table II are the downshifts obtained from this experiment and from our previous experiment.[4] From Table II, we see that: (1) low bombarding energy causes more downshift in the peak momentum than high bombarding energy for same system; (2) for the same projectile at the same bombarding energy, the peak momentum shifts more for a heavy target than for a light target; and (3) the momentum downshift for an equal-mass system of heavy nuclei is greater than that for an equal-mass system of light nuclei at the same bombarding energy.

The energy loss of the beam in the target introduces a dispersion in the energy per nucleon of the projectile. From the thickness of the target, this dispersion (standard deviation) was estimated to be 15 MeV for Nb-Nb collisions and 28 MeV for Au-Au collisions. The downshift of 30±5 (44±4) MeV/c listed in Table II for Nb-Nb (Au-Au) collisions at 800 MeV/nucleon in the rest frame of the projectile corresponds to a momentum downshift of 56±9 (81±7) MeV/c and a kinetic energy downshift of 47±8 (69±6) MeV in the laboratory; hence, we see that the downshift in the laboratory kinetic energy is significantly larger than the dispersion in the energy per nucleon of the projectile for both Nb-Nb and Au-Au collisions.

The momentum downshift of 81±7 MeV/c in the laboratory for Au-Au collisions at 800 MeV/nucleon has the same order of magnitude as the 31 MeV/c per nucleon observed by Gerbier *et al.*[14] in the measurement of the cross section for charge pickup from Au to Hg in Au-Au collisions at 960 MeV/nucleon. The downshift shown in the inclusive neutron spectra may arise from the recoil of the projectile nucleus in a collision with a target nucleon, as suggested by Gerbier *et al.*[14] The backscattering of a target neutron from a coherent collision with multiple nucleons in the projectile appears to be a source of the high-energy neutrons in the spectra, which is the topic discussed in the next section.

TABLE II. Downshift in the peak momentum of neutrons for collisions of Nb-Nb and Au-Au at 800 MeV/nucleon and collisions of Ne-Pb and Ne-NaF at 790 and 390 MeV/nucleon. The uncertainties in the downshift for the latter collisions are estimated to be 15%.

Beam energy per nucleon E (MeV/nucleon)	System	Downshift in peak momentum of neutrons ΔP (MeV/c)
800	Nb-Nb	30±5
	Au-Au	44±4
790	Ne-NaF	8
	Ne-Pb	19
390	Ne-NaF	21
	Ne-Pb	32

B. High-energy tail

One distinct feature of the inclusive spectra from both Nb-Nb and Au-Au collisions is the large width of the third Gaussian, which is responsible for the high-energy tail. The values for the standard deviation σ_3^* of 259±22 MeV/c for Nb-Nb collisions and 279±15 MeV/c for Au-Au collisions are larger than the 205±20 MeV/c obtained previously for Ne-NaF and Ne-Pb collisions at 790 MeV/nucleon. This larger width for collisions of heavy nuclei provides support for one of the three possible origins for the third Gaussian suggested earlier; namely, we interpret the third Gaussian as collective backscattering of a neutron in the target from nucleon clusters in the projectile, and attribute its larger width for collisions of heavy nuclei in this experiment to a larger mean size of the nucleon cluster in heavy projectiles compared to a light Ne projectile in our previous experiment. This interpretation is an extension of that suggested by Fujita[15] and by Fujita and Hufner,[16] who assumed the existence of "correlated clusters" to explain inclusive proton spectra at 180° measured by Frankel *et al.*[17] from collisions of 600 and 800 MeV protons on various nuclei. Here we note that Amado and Woloshyn[18] and Frankel[19] attempted to account for backward emission of high-momentum protons in proton-nucleus interactions as a single scattering of the incident protons from nucleons with very high momenta in the target nucleus; however, predictions based on this simple mechanism disagreed with measurements of the analyzing power from deuterium[20] and other nuclei[21] (Li, Be, C, and Ta) for 800 MeV polarized protons. Frankel and Frati[22] accounted for the analyzing powers observed for high-energy protons in the backward direction and for the angular distributions[23] of backward protons emitted from $(p,2p)$ reactions in terms of quasifree p-p forward scattering, which dominates the inclusive cross section, followed by both incoherent rescattering of the proton from a single residual nucleon and coherent rescattering of the proton from two or more residual nucleons.

To estimate the mean size of the nucleon clusters in the projectile, we decomposed the third Gaussian in the region above the peak momentum in Figs. 4(a) and 5(a) into three sub-Gaussians which correspond to elastic backscattering of a neutron in the target either from a nucleon in the projectile or from a nucleon cluster with a nucleon number $N=2$ or 3. The centroid of each sub-Gaussian was fixed by the backscattering momentum of 0, 353, and 553 MeV/c associated with the elastic scattering from one, two, and three nucleons, respectively, minus the momentum downshift of the peak. The standard deviation of each of these three sub-Gaussians was taken to be equal to the standard deviation σ_2 of the second Gauss-

ian. This choice for the standard deviation was based on the assumption that the uncertainty in the momentum of each of the nucleons involved in the elastic backscattering process for equal-mass systems is equal to the standard deviation σ_2 that reflects the Fermi momentum in the projectile; then, from kinematics for elastic scattering of a neutron in the target from a single neutron or a cluster of two or three nucleons in the projectile and from the propagation of uncertainties, the uncertainties in the above elastic backscattering momenta were estimated to be equal to the standard deviation σ_2. The fit yielded the amplitudes of the three sub-Gaussians. When the third Gaussian in Figs. 4(a) and 5(a) is replaced by the sub-Gaussians obtained from the fit, the envelope in the region above the peak momentum matches the data well with an insignificant difference from the match with the third Gaussian. This replacement is shown in Figs. 4(b) and 5(b) for Nb-Nb and Au-Au collisions, respectively, with the sub-Gaussians denoted by the dotted lines. From the amplitudes of the three sub-Gaussians, we found that backscattering of a target neutron from two-nucleon and three-nucleon clusters in the projectile together was about one third of that from a single nucleon in Nb-Nb and Au-Au collisions. Also, we estimated the mean size of the nucleon clusters in the projectile to be about 1.3 for both Nb and Au. The same fit was carried out also for our previous experiment with a Ne projectile; in this case, backscattering from two-nucleon and three-nucleon clusters together amounted to about 10% of that from a single nucleon, and the mean size of the nucleon clusters was about 1.1 for 390 and 790 MeV/nucleon Ne projectiles colliding with an equal mass target (viz., NaF) and a heavy target (viz., Pb). From the previous calculation, we see that the high-energy tail, which is represented by the third Gaussian, can be explained simply as collective backscattering of a neutron in the target from a cluster of nucleons in the projectile alone, and that the width of the third Gaussian reflects the mean size of the nucleon cluster in the projectile. Also, this interpretation appears reasonable in terms of the magnitude of the total cross section for elastic scattering of a target neutron from nucleon pairs in the projectile. This total cross section can be shown to be proportional to the product of the amplitude and the mean momentum of the second sub-Gaussian. We estimated that this total cross section for Au was nearly five times that for Nb; however, the cross section per target neutron from nucleon pairs was about two times larger for Au than for Nb. The magnitude of these cross sections was overestimated because of the assumption of isotropy. In comparison with the total cross section of about 12 mb for elastic scattering of an 800 MeV proton from the deuteron,[24] the number of two-nucleon clusters is less than six in the Au projectile and less than three in the Nb projectile. This result is not an unreasonable expectation particularly since knowledge of the two-nucleon cluster probability is needed for more detailed interpretation. The elastic backscattering of a target neutron from a nucleon cluster with four or more nucleons in the projectile and the quasielastic backscattering of a target proton from the projectile nucleus, together with charge exchange of the target proton with a projectile neutron, as discussed by Gerbier *et al.*,[14] would produce neutrons of kinetic energy beyond 2.5 GeV and up to about 5 Gev in the laboratory. The total cross section for these two processes is too small to measure in this experiment; however, a very rough extrapolation from the analysis of our data indicates that this total cross section is of the order of 10 mb for Au-Au collisions at 800 MeV/nucleon, which is consistent with the total cross section of 35 ± 8 mb measured by Gerbier *et al.*[14] for charge pick up from Au to Hg in the interactions at 960 MeV/nucleon.

Although this interpretation can explain the neutron observations, it does not explain the weak dependence of the width of the broad Gaussian on the mass of the target found by Geaga *et al.*[25] from measurements of inclusive proton spectra at 180° from collisions of 1.05 GeV proton on targets of mass number up to 200; nor does it explain the smaller width of 200 ± 5 MeV/c for the standard deviation of this Gaussian in the proton spectra from the heaviest targets. In our experiment, the value of σ_3^* was extracted from the Lorentz-invariant cross section, which is the product of the neutron energy and the double differential cross section; whereas, the value of Geaga *et al.* was extracted from the double differential cross section alone. In the high-momentum region where the primary contribution to the cross section comes from the process of the third Gaussian, the higher neutron energy increases the value of σ_3^* extracted from the Lorentz-invariant cross section by about 9 MeV/c for Nb-Nb collisions and 13 MeV/c for Au-Au collisions over the value that would be extracted from the double differential cross section; however, by itself, this increase is not sufficient to explain the discrepancy between the results of 259 ± 22 MeV/c for Nb-Nb collisions and 279 ± 15 MeV/c for Au-Au collisions from our measurement and the maximum value of 200 ± 5 MeV/c obtained by Geaga *et al.* from the measurement of inclusive proton spectra at 180°. Other contributions to this discrepancy might be the neglect of the downshift ΔP during the fit by Geaga *et al.* and the effect of the Coulomb interaction in the measurement of the proton spectrum. Still another possibility is that compression in heavy-ion collisions affects the neutron result.

The first of the three possible origins of the high-energy tail (viz., collective behavior from central collisions) may be weakened by the fact that the third Gaussian still appears for peripheral collisions although with a smaller amplitude. Later in this paper, we will demonstrate the appearance of the third Gaussian for peripheral collisions. If the second possible origin (viz., the high-momentum components of a Fermi distribution at a finite temperature) accounts for the high-energy tail, then the larger width of the third Gaussian for heavy projectiles implies that the Fermi distribution for heavy projectiles is associated with a higher temperature than that for light projectiles.

IV. BOUNCE OFF AND TRANSVERSE MOMENTUM OF NEUTRONS

Collective flow of nuclear matter was observed in nucleus-nucleus collisions.[26–28] One of the two collective

effects is the bounce off of spectator fragments. Inclusive measurements are not expected to reveal the bounce off effect; nevertheless, we examined the distribution of neutrons along the vertical dimension of the detector at 0° with a position resolution of less than 3 cm. In the laboratory frame, the x and y axes were defined by the horizontal and vertical dimension of the detector, respectively, and the z axis pointed from the target to the center of the detector. We measured the y coordinate of each neutron with a kinetic energy in an interval of ±30 MeV about the peak shown in Fig. 2. Most of the neutrons in this narrow energy region were evaporation neutrons. Then, from the measured y coordinate, we calculated the transverse momentum P_y of the neutrons along the y axis, which is the same in the laboratory frame and in the rest frame of the projectile. The relative number of counts from Nb-Nb collisions is plotted in Fig. 6(a) versus the transverse momentum P_y. Figure 6(b) is a similar plot for Au-Au collisions. In Fig. 6 the counts drop drastically at the two momenta which correspond to the two edges of the detector. A Gaussian fit to each of the two distributions between ±48 MeV/c yielded the standard deviation σ_{P_y} for the distribution of transverse momentum along the y axis to be 48±3 MeV/c for Nb-Nb collisions and 43±2 MeV/c for Au-Au collisions. The fit is denoted by the solid lines in Fig. 6. The standard deviation σ_{P_x} of the distribution of the transverse momentum along the x axis was equal to σ_{P_y} because of symmetry. Within uncertainties, the standard deviation σ_{P_y} is equal to the standard deviation σ_1^* of 55±4 MeV/c for Nb-Nb collisions; whereas that for Au-Au collisions is 13±5 MeV/c less than the standard deviation σ_1^* of 56±4 MeV/c for Au-Au collisions. Because the standard deviation σ_1^* is a measure of the dispersion of the longitudinal momentum P_z of evaporation neutrons in the rest frame of the projectile, the above facts indicate that the dispersion of the transverse momentum of the neutrons at 0° is determined mainly by neutron evaporation. A neutron detected at 4° must have a minimum transverse momentum P_x of about 100 MeV/c, which is about twice the value of the standard deviation σ_{P_x}. This fact implies that a superposition of a peak from neutron evaporation above an exponential curve is expected to be seen in the inclusive neutron spectra at 4°.

It is assumed that the bounce off effect, which causes the average transverse momentum of fragments in the reaction plane to deviate from 0 MeV/c, will result in a broader distribution of the neutron momentum along the y axis than that along the z axis; however, because the projection of the average transverse momentum onto the y axis for events with a random orientation of the reaction plane is, on the average, only $2/\pi$ times the value in the reaction plane, the random orientation of the reaction plane weakens the bounce off effect by a factor of about $\pi/2$. The quadrature combination of the standard deviation σ_1^* with the dispersion arising from the weakened bounce off increases the standard deviation σ_1^* by less than 10 MeV/c for a bounce off momentum with a typical value of 50 MeV/c. This estimate may be too large, and the actual difference between the width of the transverse momentum distribution of neutrons and that along the z direction may be too small to be observed in this experiment.

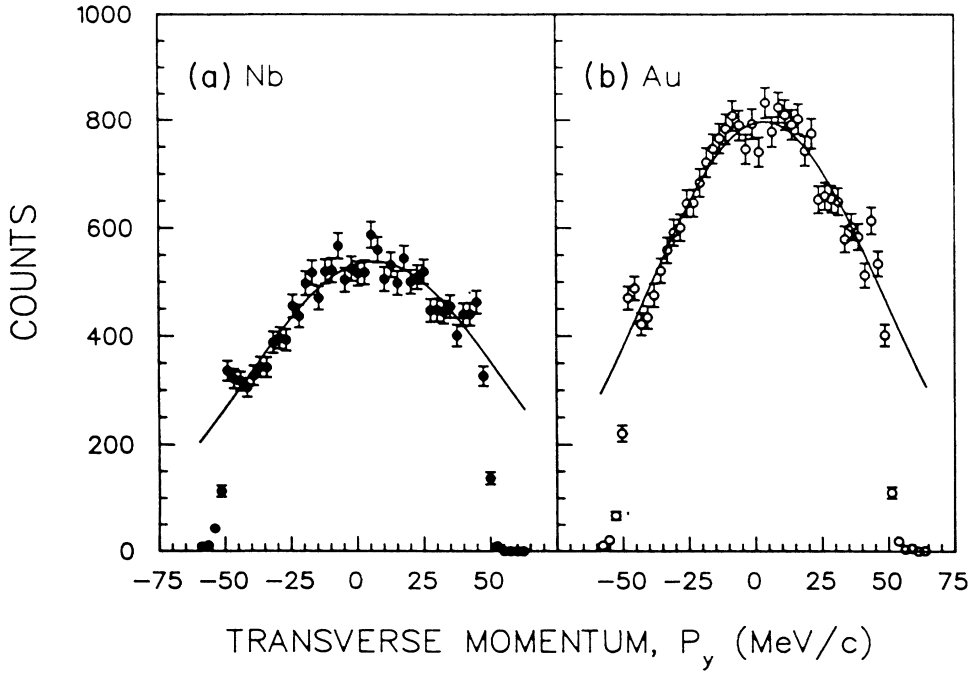

FIG. 6. The relative number of counts from (a) Nb-Nb and (b) Au-Au collisions at 800 MeV/nucleon vs the transverse momentum of neutrons with kinetic energies from 730 to 790 MeV measured along the vertical dimension of the detector at 0°. The error bars reflect statistical uncertainties only.

V. DEPENDENCE ON THE IMPACT PARAMETER

We examined the dependence of the cross-section spectrum on the impact parameter by assigning an average impact parameter to each of two impact parameter regions, which were chosen according to the pulse height determined in the centrality detector in front of the beam dump. The pulse height in the centrality detector is related to the impact parameter. Large pulse heights are associated with low-multiplicity (preferentially peripheral) collisions and small pulse heights with high-multiplicity (preferentially nonperipheral) collisions as shown by Lu *et al.*[29] Figure 7 shows a typical spectrum of this pulse height for Au-Au collisions. In Fig. 7, pulse heights in region I correspond to peripheral collisions with large impact parameters; those in region II, to nonperipheral collisions with small impact parameters. The two regions were cut at pulse heights such that collisions of each impact parameter group contributed approximately 40% to the Lorentz-invariant cross section integrated over the momentum in the rest frame of the projectile. Then, based on the assumption that the differential cross section is proportional to the square of the impact parameter b, the average impact parameter $\bar{b}$ for peripheral and nonperipheral collisions, respectively, was estimated to be 0.89 and 0.43 (in units of $2R$, where R is the radius of the Nb or Au nucleus). For each of the two impact parameter groups, the spectrum of the Lorentz-invariant cross section was decomposed into three Gaussians in the same manner as that in Figs. 4 and 5; the χ^2 per degree of freedom ranged from 0.2 to 1.3. The two subspectra and the corresponding fits are shown together in Fig. 8 for both Nb-Nb and Au-Au collisions. The solid and dashed lines in Fig. 8 have the same meanings as in Figs. 4(a) and 5(a).

The standard deviations σ_1, σ_2, and σ_3 and the amplitudes H_1, H_2, and H_3 were obtained from the Gaussians fitted to the subspectra. Listed in Table III are the standard deviations σ^* (after unfolding the momentum resolution) and the amplitudes H for both Nb-Nb and Au-Au collisions. Also listed in Table III is the sum of the three amplitudes $\sum_{i=1}^{3} H_i$ for each of the two impact parameter groups. This sum is just the cross section of the whole impact parameter group because the amplitude H_i is the Lorentz-invariant cross section of the ith process of neutron emission integrated over the momentum. As a result of the choice of the pulse height defining the two regions shown in Fig. 7, the sum for each impact parameter group is the same, within uncertainties, with the sum for

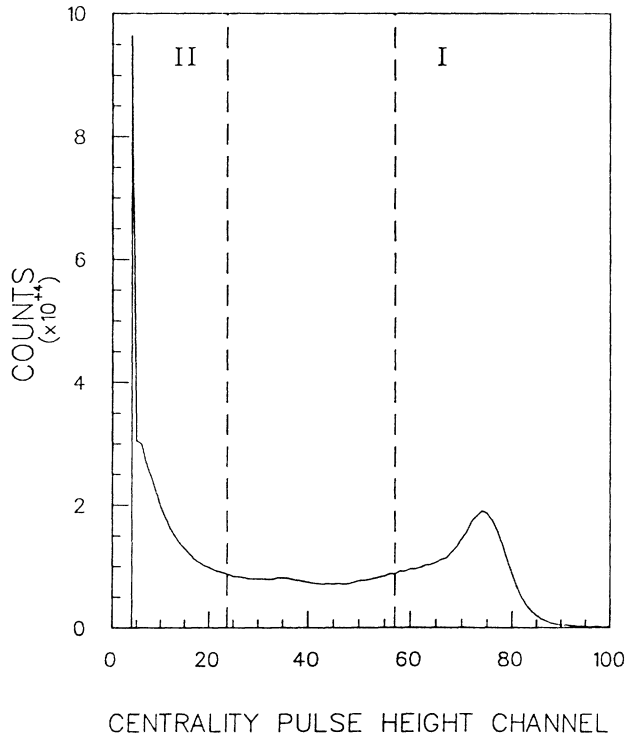

FIG. 7. A typical spectrum of the pulse height in the centrality detector for Au-Au collisions at 800 MeV/nucleon. The abscissa is compressed from the original 4000 channels to 100 channels. Region I and region II each contribute approximately 40% to the cross section. The average impact parameter $\bar{b}/2R$ is 0.89 in region I and 0.43 in region II. The broad peak at large pulse heights in region I comes from the atomic number of the projectile as a result of very peripheral collisions which disturb the projectile only slightly; the sharp peak at small pulse heights in region II corresponds to light nuclei as a result of nonperipheral collisions which leave these ions in the beam.

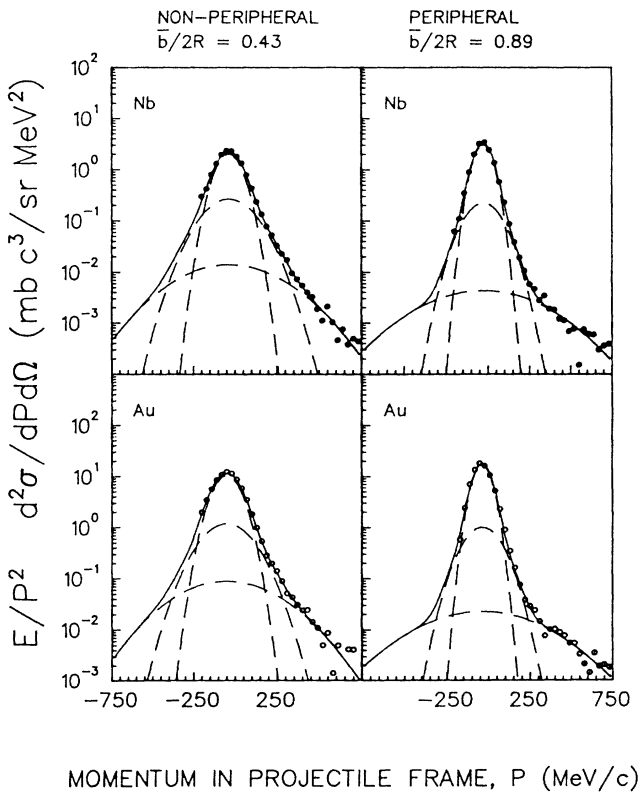

FIG. 8. The Lorentz-invariant cross section at 800 MeV/nucleon for neutron emission at 0° from Nb-Nb and Au-Au collisions for small and large impact parameter groups vs the neutron momentum in the rest frame of the projectile.

TABLE III. Parameters of the three Gaussians in the decomposition of the neutron subspectra at 0° in the rest frame of the projectile from the two impact parameter groups of Nb-Nb and Au-Au collisions at 800 MeV/nucleon.

System	Average impact parameter $\bar{b}/2R$	Gaussian	Standard deviation σ (MeV/c)	Amplitude H (mb c^2/sr MeV)	Sum of three amplitudes $\sum_{i=1}^{3} H_i$ (mb c^2/sr MeV)
Nb-Nb	0.43	1	67±4	332±34	428±49
		2	133±15	87±36	
		3	271±41	9±7	
	0.89	1	49±3	375±30	430±37
		2	95±8	52±21	
		3	307±39	3±1	
Au-Au	0.43	1	71±4	1701±143	2101±226
		2	128±15	347±174	
		3	263±27	53±22	
	0.89	1	48±5	1863±129	2098±168
		2	96±6	219±88	
		3	316±27	16±3	

Au-Au collisions being about five times that for Nb-Nb collisions. Within the uncertainties, the values of σ_3^* for each of the two impact parameter groups in Table III agree with each other and also with the value of σ_3^* in Table I for inclusive collisions. This result indicates that the third Gaussian originates from both nonperipheral and peripheral collisions. The values of both σ_1^* and σ_2^* are smaller for collisions with large impact parameters than for collisions with small impact parameters. The evaporation temperatures T_e extracted from the σ_1^* are 4.8±0.6 and 2.6±0.3 MeV (5.4±0.6 and 2.5±0.5 MeV) for Nb-Nb (Au-Au) collisions with small and large impact parameters, respectively. The evaporation temperature decreases for peripheral collisions. The decrease in the value of σ_2^* indicates that the momentum distribution of neutrons knocked out from the projectile is narrower for peripheral collisions than for nonperipheral collisions; qualitatively, peripheral collisions sample nucleons near the nuclear surface, whereas nonperipheral collisions tend to sample interior nucleons which are bound more tightly.

From the amplitudes H for both Nb-Nb and Au-Au collisions, we calculated the following fractions: $F_i = H_i / \sum_{i=1}^{3} H_i$ with $i = 1$ to 3. These fractions are listed in Table IV. They reflect the contributions to the cross section from the three processes. Examination of the fractions in Table IV reveals the following results. First, for a given impact parameter group, the fractions are the same within uncertainties for both the Au-Au and Nb-Nb systems even though the amplitudes H_i for Au-Au collisions are typically four to five times as large as those for Nb-Nb collisions. Second, within uncertainties, neither the fraction F_1 nor the fraction F_2 reveals a significant change with the average impact parameter. Third, we see that the fraction F_3 of 2.5±1.0 % for Au-Au collisions with small impact parameters is larger than that of 0.8±0.2 % for collisions with large impact parameters, the difference being 1.7±1.0 %. For Nb-Nb collisions, there is no significant difference between the two fractions of 2.2±1.7 % and 0.8±0.3 % for small and large impact parameter groups; the large uncertainty here arises because of the low statistics of the Nb-Nb data. The ratio of the contribution to the third Gaussian from nonperipheral collisions with small impact parameters to that from peripheral collisions with large impact parameters is 3.1±1.5 for Au-Au collisions and 2.8±2.4

TABLE IV. Percentage contribution from each of the three processes of neutron emission to the cross section at 0° for 800 MeV/nucleon Nb-Nb and Au-Au collisions for two impact parameter groups.

System	Average impact parameter $\bar{b}/2R$	Percentage contribution from each process F_1	F_2	F_3
Nb-Nb	0.43	77.6±7.0	20.2±7.2	2.2±1.7
	0.89	87.1±4.4	12.1±4.4	0.8±0.3
Au-Au	0.43	81.0±6.9	16.5±7.0	2.5±1.0
	0.89	88.8±3.7	10.5±3.7	0.8±0.2

for Nb-Nb collisions. This result, especially for the Au-Au system, indicates that the process represented by the third Gaussian comes primarily from nonperipheral collisions; hence, nonperipheral collisions constitute the primary source of the high-energy tail of the neutron spectrum.

VI. CONCLUSIONS

We measured inclusive neutron spectra at 0° from collisions of 800 MeV/nucleon Nb on Nb and Au on Au. Three processes of neutron emission are distinguished by the Lorentz-invariant cross section at 0° in the rest frame of the projectile: the excitation and evaporative decay of the projectile spectator, the fragmentation of a neutron from the projectile, and the elastic backscattering of a neutron in the target from a cluster of nucleons in the projectile. The neutron evaporation temperature in the projectile is insensitive to the mass of the projectile in collisions with a target of equal mass. The extracted Fermi momentum agrees with predictions of statistical models, and (within uncertainties) with those extracted from quasielastic electron scattering. High-energy neutrons appear in both peripheral and nonperipheral collisions, but come primarily from nonperipheral collisions. Elastic backscattering of a target neutron from two- and three-nucleon clusters can account for the high-energy neutrons. The mean size of neutron cluster in the projectile is 1.3 for Au and Nb and 1.1 for Ne. The cross section for elastic backscattering of a target neutron from a two-nucleon cluster in the projectile is reasonable in comparison with the world average of the cross section for elastic scattering of a proton from the deuteron. The results indicate also that the evaporation temperature increases with decreasing impact parameter, that the width of the momentum distribution of a neutron in the projectile increases for collisions with decreasing impact parameter, which means that the neutrons involved in nonperipheral collisions have a broader momentum distribution than those involved in peripheral collisions, and that the width of the Gaussian reflecting elastic backscattering is independent of the impact parameter. An analysis of the distribution of the transverse momentum of the evaporation neutrons in this experiment shows that these inclusive measurements do not provide an effective way to study the bounce off of spectator neutrons.

This work was supported in part by the National Science Foundation and the U.S. Department of Energy.

---

*Present address: University of Maryland, College Park, MD 20742.

†Present address: Fast Neutron Research Facility, Chiang Mai University, Chiang Mai 50002, Thailand.

[1]H. Feshbach and K. Huang, Phys. Lett. **47B**, 300 (1973).

[2]A. S. Goldhaber, Phys. Lett. **53B**, 306 (1974).

[3]H. H. Heckman, D. E. Greiner, P. J. Lindstrom, and F. S. Bieser, Phys. Rev. Lett. **28**, 926 (1972).

[4]R. Madey *et al.*, Phys. Rev. Lett. **55**, 1453 (1985).

[5]A. R. Baldwin and R. Madey, Nucl. Instrum. Methods **171**, 149 (1980).

[6]R. Madey *et al.*, Nucl. Instrum. Methods **214**, 401 (1983).

[7]R. A. Cecil, B. D. Anderson, and R. Madey, Nucl. Instrum. Methods **161**, 439 (1979).

[8]B. D. Anderson, J. N. Knudson, R. Madey, and C. C. Foster, Nucl. Instrum. Methods **169**, 153 (1980).

[9]S. Cierjacks *et al.*, Nucl. Instrum. Methods **192**, 407 (1982).

[10]J. W. Watson *et al.*, Nucl. Instrum. Methods **215**, 413 (1983).

[11]J. D'Auria *et al.*, Phys. Rev. C **30**, 1999 (1984).

[12]R. Jeppesen, Ph.D. dissertation, University of Colorado, 1986.

[13]E. J. Moniz *et al.*, Phys. Rev. Lett. **26**, 445 (1971).

[14]G. Gerbier, Ren Guoxiao, and P. B. Price, Phys. Rev. Lett. **60**, 225 (1988).

[15]T. Fujita, Phys. Rev. Lett. **39**, 174 (1977).

[16]T. Fujita and J. Hufner, Nucl. Phys. **A314**, 317 (1979).

[17]S. Frankel, W. Frati, O. Van Dyck, R. Werbeck, and V. Highland, Phys. Rev. Lett. **36**, 642 (1976).

[18]R. D. Amado and R. M. Woloshyn, Phys. Rev. Lett. **36**, 1435 (1976).

[19]S. Frankel, Phys. Rev. Lett. **38**, 1338 (1977).

[20]H. Brody, S. Frankel, W. Frati, and O. B. Van Dyck, Phys. Rev. C **24**, 2157 (1981).

[21]S. Frankel *et al.*, Phys. Rev. Lett. **41**, 148 (1978); S. Frankel *et al.*, University of Pennsylvania Report No. UPR-0050N, 1977 (unpublished).

[22]S. Frankel and W. Frati, Phys. Rev. C **24**, 2739 (1981).

[23]S. Frankel, W. Frati, C. F. Perdrisat, and O. B. Van Dyck, Phys. Rev. C **24**, 2684 (1981).

[24]Particle Data Group, Phys. Lett. **170B**, 89 (1986).

[25]J. Geaga *et al.*, Phys. Rev. Lett. **45**, 1993 (1980).

[26]H. A. Gustafsson *et al.*, Phys. Rev. Lett. **52**, 1590 (1984).

[27]R. E. Renfordt *et al.*, Phys. Rev. Lett. **53**, 763 (1984).

[28]D. Beavis *et al.*, Phys. Rev. C **27**, 2443 (1983); Phys. Rev. Lett. **54**, 1652 (1985).

[29]J. J. Lu *et al.*, Phys. Rev. Lett. **46**, 898 (1981).